First laser emission of $Yb_{0.15}:(Lu_{0.5}Y_{0.5})_3Al_5O_{12}$ ceramics

Guido Toci,[1] Angela Pirri,[2,*] Jiang Li,[3] Tengfei Xie,[3] Yubai Pan,[3] Vladimir Babin,[4] Alena Beitlerova,[4] Martin Nikl,[4] and Matteo Vannini[1]

[1]*C.N.R. - National Research Council, Istituto Nazionale di Ottica, Via Madonna del Piano 10, I-50019 Sesto Fiorentino (FI), Italy*

[2]*C.N.R. - National Research Council, Istituto di Fisica Applicata "Nello Carrara" Via Madonna del Piano 10, I-50019 Sesto Fiorentino (FI), Italy*

[3]*Key Laboratory of Transparent and Opto-functional Advanced Inorganic Materials, Shanghai Institute of Ceramics, Chinese Academy of Sciences, 1295 Dingxi Road, Shanghai 200050, China*

[4]*Institute of Physics Academy of Sciences of the Czech Republic, Cukrovarnicka 10, Prague 162 53, Czech Republic*

[*]*a.pirri@ifac.cnr.it*

Abstract: We report the first laser oscillation on $Yb_{0.15}:(Lu_{0.5}Y_{0.5})_3Al_{12}$ ceramics at room temperature. At 1030 nm we measured a maximum output power of 7.3 W with a corresponding slope efficiency of 55.4% by using an output coupler with a transmission of T = 39.2%. The spectroscopic properties are compared with those of the two parent garnets Yb:YAG and Yb:LuAG. To the best of our knowledge these are the first measurements reported in literature achieved with this new host.

©2016 Optical Society of America

OCIS codes: (140.0140) Lasers and laser optics; (140.3615) Lasers, ytterbium; (140.3580) Lasers, solid-state; (140.5680) Rare earth and transition metal solid-state lasers; (140.3600) Lasers, tunable; (160.3380) Laser materials.

References and links

1. L. D. DeLoach, S. A. Payne, L. L. Chase, L. K. Smith, W. L. Kway, and W. F. Krupke, "Evaluation of absorption and emission properties of Yb^{3+} doped crystals for laser applications," IEEE J. Quantum Electron. **29**(4), 1179–1191 (1993).
2. F. Druon, S. Ricaud, D. N. Papadopoulos, A. Pellegrina, P. Camy, J. L. Doualan, R. Moncorgé, A. Courjaud, E. Mottay, and P. Georges, "On Yb:CaF_2 and Yb:SrF_2: review of spectroscopic and thermal properties and their impact on femtosecond and high power laser performance [Invited]," Opt. Mater. Express **1**(3), 489–502 (2011).
3. A. Pirri, G. Toci, and M. Vannini, "First laser oscillation and broad tunability of 1 *at.* % Yb-doped Sc_2O_3 and Lu_2O_3 ceramics," Opt. Lett. **36**(21), 4284–4286 (2011).
4. A. Pirri, M. Vannini, V. Babin, M. Nikl, and G. Toci, "CW and quasi-CW laser performance of 10 *at.*% Yb^{3+}:LuAG ceramic," Laser Phys. **23**(9), 095002 (2013).
5. F. Tang, Y. G. Cao, J. Q. Huang, W. Guo, H. G. Liu, W. C. Wang, Q. F. Huang, and J. T. Li, "Diode-pumped multilayer Yb:YAG composite ceramic laser," Laser Phys. Lett. **9**(8), 564–569 (2012).
6. M. Tsunekane and T. Taira, "High-power operation of diode edge-pumped, composite all ceramic Yb:$Y_3Al_5O_{12}$ microchip laser," Appl. Phys. Lett. **90**(12), 121101 (2007).
7. A. A. Kaminskii, M. Sh. Akchurin, R. V. Gainutdinov, K. Takaichi, A. Shirakava, H. Yagi, T. Yanagitani, and K. Ueda, "Microhardness and Fracture Toughness of Y_2O_3- and $Y_3Al_5O_{12}$-Based Nanocrystalline Laser Ceramics," Crystallogr. Rep. **50**(5), 935–939 (2005).
8. Y. Kuwano, K. Suda, N. Ishizawa, and T. Yamada, "Crystal growth and properties of $(Lu,Y)_3Al_5O_{12}$," J. Cryst. Growth **260**(1-2), 159–165 (2004).
9. S. Cheng, X. Xu, D. Li, D. Zhou, F. Wua, Z. Zhao, and J. Xu, "Growth and spectroscopic properties of Yb:$Lu_{1.5}Y_{1.5}Al_5O_{12}$ mixed crystal," Opt. Mater. **33**(1), 112–115 (2010).
10. F. Wang, Z. Qin, G. Xie, P. Yuan, L. Qian, X. Xu, and J. Xu, "8.5 W mode-locked Yb:$Lu_{1.5}Y_{1.5}Al_5O_{12}$ laser with master oscillator power amplifiers," Appl. Opt. **54**(5), 1041–1045 (2015).
11. M. Sun, J. Y. Long, X. H. Li, Y. Liu, H. F. Ma, Y. An, X. H. Hu, Y. S. Wang, C. Li, and D. Y. Shen, "Widely tunable Tm:LuYAG laser with a volume Bragg grating," Laser Phys. Lett. **9**(8), 553–556 (2012).
12. X. F. Yang, Y. Wang, D. Y. Shen, T. Zhao, X. D. Xu, D. H. Zhou, and J. Xu, "Efficient Er:LuYAG laser operating at 1648 and 1620 nm," Laser Phys. Lett. **9**(2), 131–134 (2012).
13. J. Q. Di, X. D. Xu, D. Z. Li, D. H. Zhou, F. Wu, Z. W. Zhao, J. Xu, and D. Y. Tang, "CW Laser Properties of Nd:GdYAG, Nd:LuYAG, and Nd:GdLuAG Mixed Crystals," Laser Phys. **21**(10), 1742–1744 (2011).
14. G. Toci, "Lifetime measurements with the pinhole method in presence of radiation trapping: I-theoretical model," Appl. Phys. B **106**(1), 63–71 (2012).
15. G. Toci, D. Alderighi, A. Pirri, and M. Vannini, "Lifetime measurements with the pinhole method in presence of radiation trapping: II-application to Yb^{3+} doped ceramics and crystals," Appl. Phys. B **106**(1), 73–79 (2012).

#253527 Received 6 Nov 2015; revised 10 Dec 2015; accepted 10 Dec 2015; published 25 Apr 2016
© 2016 OSA

16. B. F. Aull and H. P. Jenssen, "Vibronic interaction Nd:YAG resulting in non reciprocity of absorption and stimulated emission cross section," IEEE J. Quantum Electron. **18**(5), 925–930 (1982).
17. R. Gaume, B. Viana, D. Vivien, J. P. Roger, and D. Fournier, "A simple model for the prediction of thermal conductivity in pure and doped insulating crystals," Appl. Phys. Lett. **83**(7), 1355–1357 (2003).
18. A. Pirri, D. Alderighi, G. Toci, and M. Vannini, "High-efficiency, high-power and low threshold Yb^{3+}:YAG ceramic laser," Opt. Express **17**(25), 23344–23349 (2009).
19. A. Brenier, Y. Guyot, H. Canibano, G. Boulon, A. Ródenas, D. Jaque, A. Eganyan, and A. G. Petrosyan, "Growth, spectroscopic and laser properties of Yb^{3+}-doped $Lu_3Al_5O_{12}$ garnet crystal," J. Opt. Soc. Am. B **23**(4), 676–683 (2006).
20. K. Beil, S. T. Fredrich-Thornton, F. Tellkamp, R. Peters, C. Kränkel, K. Petermann, and G. Huber, "Thermal and laser properties of Yb:LuAG for kW thin disk lasers," Opt. Express **18**(20), 20712–20722 (2010).
21. M. Nikl, A. Yoshikawa, and T. Fukuda, "Charge transfer luminescence in Yb^{3+}-containing compounds," Opt. Mater. **26**(4), 545–549 (2004).
22. H. Kühn, S. T. Fredrich-Thornton, C. Kränkel, R. Peters, and K. Petermann, "Model for the calculation of radiation trapping and description of the pinhole method," Opt. Lett. **32**(13), 1908–1910 (2007).
23. A. Caird, S. A. Payne, P. R. Staver, A. J. Ramponi, and L. L. Chase, "Quantum electronic properties of the $Na_3Ga_2Li_3F_{12}$: Cr^{3+} laser," IEEE J. Quantum Electron. **24**(6), 1077–1099 (1988).
24. J. Koerner, C. Vorholt, H. Liebetrau, M. Kahle, D. Kloepfel, R. Seifert, J. Hein, and M. C. Kaluza, "Measurement of temperature-dependent absorption and emission spectra of Yb:YAG, Yb:LuAG, and Yb:CaF_2 between 20 °C and 200 °C and predictions on their influence on laser performance," J. Opt. Soc. Am. B **29**(9), 2493–2502 (2012).
25. A. Pirri, G. Toci, D. Alderighi, and M. Vannini, "Effects of the excitation density on the laser output of two differently doped Yb:YAG ceramics," Opt. Express **18**(16), 17262–17272 (2010).
26. A. Pirri, G. Toci, M. Nikl, V. Babin, and M. Vannini, "Experimental evidence of a nonlinear loss mechanism in highly doped Yb:LuAG crystal," Opt. Express **22**(4), 4038–4049 (2014).

1. Introduction

The interest on Yb doped solid state materials has steadily grown over the last decade. This success is due to the presence of several interesting features that make them suitable for high power and high efficiency laser devices [1,2]. The large availability of hosts for Yb^{3+} provides a broad variability in the spectroscopic, optical and thermomechanical properties, with the possibility of finely tuning the choice of the material according to the specific application needs. The availability of new hosts is further widened by the development of transparent polycrystalline ceramics. The ceramic fabrication methods usually require lower processing temperatures than crystal growth techniques, providing a more convenient approach for the fabrication of materials with high melting point such as sesquioxides and some garnets [3,4]. Moreover ceramics are better suited than single crystals for the fabrication and structuring of large gain elements for high power applications [5,6], and at least in some cases they exhibit a higher mechanical resistance [7].

In this paper we report on the fabrication, the spectroscopic properties and the laser performance of Yb-doped mixed garnet ceramics, namely $Yb_{0.15}:(Lu_{0.5}Y_{0.5})_3Al_5O_{12}$ (hereafter Yb:LuYAG). To the best of our knowledge, this is the first time that laser emission is demonstrated for Yb-doped LuYAG ceramics.

The use of these Lu and Y garnets as laser hosts was firstly proposed by Kuwano *et al*. [8]. There are several motivations for their use as laser hosts, in relation to its "parent" garnets (*i.e.* YAG and in particular LuAG): the disordered crystal structure resulting from the mixing of the two composition could induce a spectral broadening and/or a spectral shift of the absorption and the emission band of several dopants, providing a broader tuning range or emission wavelengths well suited for specific applications; the melting point of the LuYAG is lower than LuAG by several tens of K, resulting in an easier crystal growth; the preparation of LuYAG in comparison with LuAG requires a smaller amount of high purity Lu_2O_3 powder, which is very expensive. On the other hand LuYAG has a high thermal conductivity [8], similar to LuAG, which should be almost unaffected by Yb doping, providing an advantage over YAG at high doping levels. The first spectroscopic characterization of Yb:LuYAG crystal was carried out by Cheng *et al.* [9], and the only demonstration of laser operation (in mode-locking regime) was reported by Wang *et al.* [10]. Single crystal LuYAG was also used as laser host for other dopants, such as Tm [11], Er [12] and Nd [13].

#253527 Received 6 Nov 2015; revised 10 Dec 2015; accepted 10 Dec 2015; published 25 Apr 2016
© 2016 OSA

2. Material fabrication and spectroscopic characterization

The Yb:LuYAG ceramic samples were prepared using high purity α-Al_2O_3, Lu_2O_3, Y_2O_3, Yb_2O_3 powders as starting materials. Tetraethoxysilane (TEOS) and MgO were used as sintering aids. Powder batches were ball milled in a corundum bottle for 10 h with 10 mm diameter Al_2O_3 balls in ethanol. After ball milling, the slurry was dried, uniaxially pressed into 20 mm diameter pellets at 20 MPa, and then cold isostatically pressed at 200 MPa. Sintering was conducted at 1850 °C for 30 h in a tungsten mesh-heated vacuum furnace under 5×10^{-4} Pa vacuum during holding. After sintering, the specimens were annealed at 1500°C for 10 h in air to remove the oxygen vacancies. The resulting samples have a diameter of about 16 mm and a thickness of about 4 mm, and were then cut to a thickness of 1.4 mm and carefully polished for the laser tests. The transmission spectrum (Fig. 1(a)) was recorded at room temperature with a Shimadzu spectrometer 3101PC. The residual scattering losses in the near infrared are around 1%, corresponding to a scattering coefficient of about 0.15 cm^{-1}.

The microstructure of the fracture surface of the ceramics was observed by field emission scanning electron microscopy (FESEM, SU8220, Hitachi, Japan). It can be seen (Fig. 1(b)) that the grain boundaries are clean and there are almost no pores and secondary phase at grain boundaries or inner grains.

The lifetime of the upper laser level was measured using the so-called pinhole method [14] with an experimental set-up described in [15], to avoid radiation trapping effects. On the 15*at.*% doped sample the lifetime was 873 μs, whereas on another sample with 5*at.*% doping it resulted 935 μs. The fluorescence spectrum was excited with a semiconductor laser emitting at 936 nm, using a 90° excitation-detection geometry on the sample edge to minimize the reabsorption effects, and acquired with a grating spectrometer equipped with a CCD array (spectral resolution 1.5 nm). Pulsed excitation and delayed synchronous detection were used to reject the pump signal.

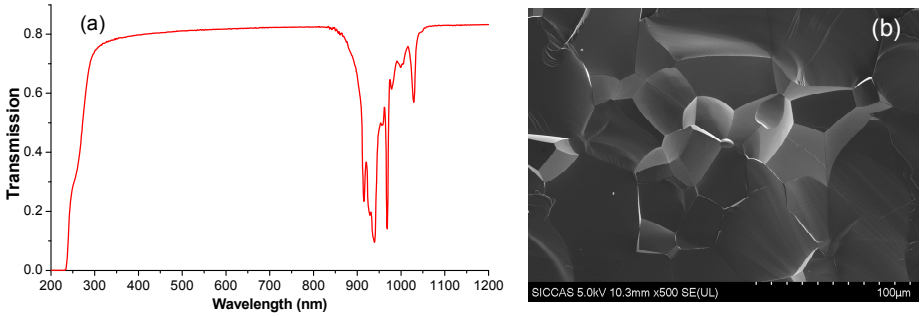

Fig. 1. (a): Transmission spectrum; (b): FESEM image of the sample fracture surface.

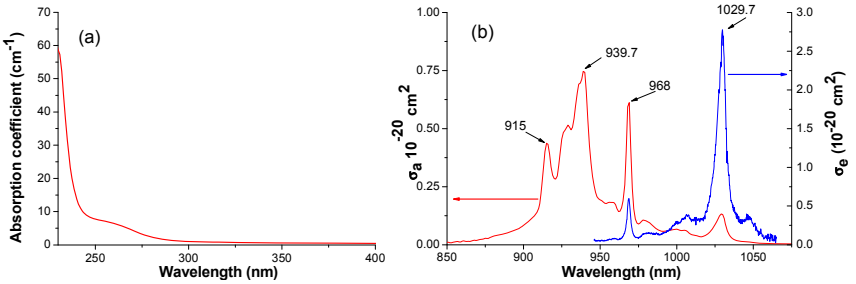

Fig. 2. (a): Absorption coefficient in the blue-UV; (b): Absorption and emission cross section spectra (σ_a and σ_e respectively) of the Yb^{3+} 4f-4f transition.

#253527 Received 6 Nov 2015; revised 10 Dec 2015; accepted 10 Dec 2015; published 25 Apr 2016
© 2016 OSA

The emission cross section spectrum was calculated with the β-τ method [16], using the lifetime value of 935 μs for the calculation. The reciprocity method was not used to infer the emission cross section spectrum because the energy levels of Yb in LuYAG are not known with sufficient accuracy. Figure 2 shows the absorption coefficient of the sample in the blue-UV (a) and the resulting absorption and emission cross section spectra (b).

The thermal conductivity in undoped LuYAG is quite constant at about 7.5 W/mK for Lu concentration in the range from 25*at.*% to 75*at.*% [8], which is lower than both undoped YAG and LuAG (13 W/mK and 10 W/mK respectively [8]) owing to the enhanced scattering of phonons due to microscopic strains introduced in the mixed crystal lattice. On the other hand it should be scarcely affected by the Yb doping, because of the similar atomic mass of Lu and Yb (see Gaume *et al.* [17]). The cation sites density was calculated by the lattice constant reported in [8]. These parameters are summarized in Table 1.

Table 1. Spectroscopic, structural and thermal properties of $Yb_{0.15}:(Lu_{0.5}Y_{0.5})_3Al_5O_{12}$

Parameter	Value	Parameter	Value
Peak absorption cross sect. (cm^2)	$7.5x10^{-21}$ (939.5 nm)	Upper level lifetime	935 μs
Peak emission cross sect. (cm^2)	$2.8x10^{-20}$ (1030.4 nm)	Refractive index	1.821 (1014 nm) [8]
FWHM of the emission peak	6.8 nm	Thermal conductivity, undoped	7.5 W/(m K) [8]
Cation sites density (cm^{-3})	$1.403x10^{22}$ (from [8])		

3. Laser tests

The laser set up used to test the laser behavior of the ceramic sample is schematically shown in Fig. 3. The sample (C) is longitudinally pumped by a laser diode emitting at 936 nm coupled to a 200 μm fiber (numerical aperture 0.22), delivering up to 21 W, whose tip is reimaged on the sample by a pair of achromatic doublets, resulting in an almost Gaussian intensity distribution (radius 150 μm at $1/e^2$). The resonator is constituted by the End Mirror (EM) which is flat with a dichroic coating (high transmission at 936 nm, high reflectivity above 1000 nm), by the Folding Mirror (FM, curvature radius 100 mm) and by the flat Output Coupler (OC). The distance between FM and OC is 220 mm, and the total resonator length is around 276 mm.

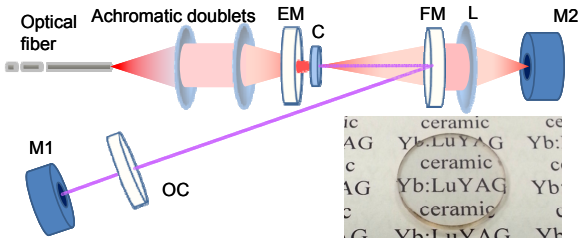

Fig. 3. Laser cavity layout. The inset shows the ceramic sample (thickness 1.4 mm, ∅ 16 mm).

The sample shown in Fig. 3 is soldered on one face with Indium on a copper heat sink (with a central hole with 3 mm diameter to let the beam pass through), water-cooled at 19°C, and it is pumped either in *quasi*-Continuous Wave (QCW, duty factor 20%, repetition rate 10 Hz) or in CW. The sample has no anti-reflection coating, consequently to minimize the impact of the Fresnel losses at the interface, the reflections were carefully realigned back on the cavity axis. The pump power not absorbed by the sample is transmitted by FM, collected by the lens L and measured by the power meter M2, allowing to determine the absorbed pump power by the sample and then the actual laser efficiency during the laser action. The unsaturated absorption of the ceramic is 80% (in QCW) and 82% (in CW). The output power is measured by the meter M1. The tunable laser cavity is obtained by replacing the OC by a gold coated grating (1800 grooves/mm) set at the Littrow's angle, using the zero order for the output coupling. The zero-order diffraction efficiency at 1030 nm is around 6% [18].

Figure 4(a) reports the output power as a function of the absorbed pump power (P_{abs}) obtained by using several OC with different transmission (from T_{OC}~2% to T_{OC}~58%); the

#253527 Received 6 Nov 2015; revised 10 Dec 2015; accepted 10 Dec 2015; published 25 Apr 2016
© 2016 OSA

slope efficiencies are reported in Fig. 4(b). The highest output power (P_{out} = 7.3 W) and slope efficiency (η_s = 55.4%) are obtained with T = 39.2%. However, remarkable results (P_{out} > 6.1 W, slope efficiency near to or exceeding 50%) are achieved for all OCs having a transmission higher than 11%. Figure 4(c) shows the output power under CW pumping, with a OC with T_{OC} = 11.8%. The decrease of the laser output power as well as the slope efficiency (P_{out} = 0.95 W with η_s = 18.3%) in comparison with the data obtained in QCW, indicates the occurrence of thermal effects. The laser threshold (~1.4 W) remain constant for all OCs, both under CW and QCW pumping. In free running the laser emitted on a single line at 1030 nm, with a linewidth of about 1.4 nm FWHM, with all OCs, both in CW and QCW. The M^2 beam quality factor in CW at a pump power of 5.7 W was 2.10 along the cavity folding plane, and 1.76 in the perpendicular direction, owing to the cavity astigmatism. The far field beam profile in CW is shown in the inset of Fig. 4(c).

Finally, we explored the tuning range measuring the output power at several wavelengths. It ranges from 1001 nm to 1054 nm (Fig. 4(d)), with a measured linewidth of 0.6 nm FWHM (limited by the spectrometer resolution); the peak output power is slightly above 1.8 W.

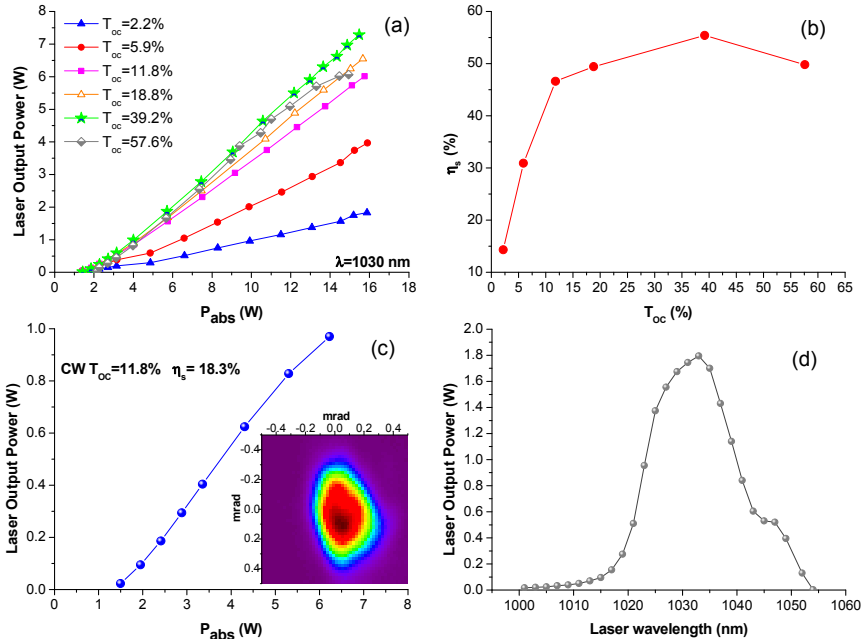

Fig. 4. (a): QCW laser output power versus the absorbed pump power; (b): Values of the slope efficiency for the various OC transmissions; (c): CW laser output power versus the absorbed pump power; the inset shows the far field beam intensity distribution at a pump power of 5.7 W; (d): Tuning range under QCW at 936 nm with an input pump power of 21.75 W.

4. Discussion

The solid-state reactive sintering method used in the preparation of the sample resulted in a very transparent material with small internal scattering losses. The absorption and emission cross section spectra have an intermediate shape between the parent garnets Yb:YAG and Yb:LuAG. The main absorption peak at 939.5 nm is slightly blue shifted with respect to YAG (941 nm, see Brenier *et al.* [19]) and similar to LuAG, but it does not feature the slight splitting that can be seen in LuAG [19]. The peak value of the absorption cross section ($7.5x10^{-21}cm^2$) is nearer to LuAG ($7.2x10^{-21}cm^2$) than to YAG ($8.2x10^{-21}cm^2$) [20]. The emission cross section spectrum has a main peak around 1030 nm, with a peak value ($2.8x10^{-20}cm^2$) which again is more similar to that of LuAG ($3.0x10^{-20}cm^2$ in [19],

#253527 Received 6 Nov 2015; revised 10 Dec 2015; accepted 10 Dec 2015; published 25 Apr 2016
© 2016 OSA

$2.59x10^{-20}cm^2$ in [20]) than to YAG ($2.14x10^{-20}cm^2$ [20]). The emission spectrum also shows a secondary peak at about 1047 nm (value about $3.6x10^{-21}cm^2$), more evident than the corresponding feature in Yb:LuAG, and similar to that shown by Yb:YAG. The measured values of emission cross section are much higher than those reported in [9] on crystalline Yb:LuYAG. The reason for this discrepancy is not yet understood.

In near ultraviolet region, the edge of the Yb^{3+} Charge Transfer Transition (CTT) can be seen at about 237 nm as well as the absorption shoulder at about 262 nm, ascribed to the Tb^{3+} impurity (4f–5d LS transition) coming from the raw Lu_2O_3 powder following [21].

The value of the upper level lifetime (935 μs on the 5% doped sample) is slightly shorter than in the parent compositions (951 μs for Yb:YAG, see Kuhn *et al.* [22], 985 μs for Yb:LuYAG [20]); the shorter lifetime (873 μs) measured on the 15% doped sample suggests the occurrence of concentration quenching effects.

The laser slope efficiency levels obtained in the QCW laser test were quite high, near or exceeding 50% for several output couplers. This indicates that the optical quality of the ceramic sample is good. Using the Caird analysis [23], from the slope efficiencies reported in Fig. 4 we evaluated that the round-trip nonsaturable internal cavity loss is 4.8%. This value is slightly higher than that expected from the sample scattering losses (around 2% over a round trip, see Section 1), and it is probably affected also by residual losses due to Fresnel reflection at the uncoated sample interfaces. Concerning with the CW pumping, the laser efficiency was lower due to the occurrence of thermal effects, less important under QCW operation. In particular, in Yb:LuAG and Yb:YAG the increase in the temperature decreases the emission cross section and increases the ground level absorption (Koerner *et al.* [24]) reducing the laser extraction. Similar thermal effects should affect Yb:LuYAG as well, because of the similar energy level structure. Besides, the occurrence of thermal lens effects cannot be neglected.

The tuning range, see Fig. 4(d), was slightly broader than 10*at.*% doped Yb:LuAG [4], due to the presence of the secondary emission peak at 1047 nm, and slightly narrower than 10*at.*% doped Yb:YAG [18], obtained using similar tuning methods.

5. Conclusions

We have characterized the spectroscopic properties and the laser emission of an Yb:LuYAG ceramics, manufactured by solid-state reactive sintering. To our knowledge, this is the first demonstration of laser emission from a ceramic with this composition.

The spectroscopic properties of the mixed garnet are intermediate between those of the parent compositions Yb:YAG and Yb:LuAG. Owing to the high optical quality, laser slope efficiencies were quite high, exceeding 50%. With a similar set-up and pumping conditions we recently obtained a maximum slope efficiency of 54% from a 10*at.*% Yb-doped YAG ceramic [18], about 60% with a 10*at.*% doped LuAG ceramics [4] and 54% from a 15*at.*% Yb-doped LuAG crystal [25]. Wang *et al.* [10] obtained a slope efficiency of 61% with an 8% doped $Yb:Lu_{1.5}Y_{1.5}Al_5O_{12}$ crystal. The slope efficiency levels here reported for Yb:LuYAG ceramics compares well with these previous results.

Considering the generation and amplification of short laser pulses, the spectral width of the main emission peak at 1030 nm could sustain a pulse duration as short as about 170 fs.

We notice here that in our previous characterization of highly doped Yb:YAG and Yb:LuAG ceramics, high inversion population levels triggered a nonlinear loss mechanism leading to a sudden decrease of the laser efficiency [25, 26]. In the sample under test we did not observe such a behaviour, despite the similar excitation density levels and thermal conditions. We will further investigate on this subject.

Acknowledgments

This work was supported by CNR-AVCR Joint Project 2013-2015 “Influence of composition and defects on the properties of transparent ceramics and crystals for laser and scintillator applications” and also partially supported by the National Natural Science Foundation of China (Grant No. 61575212) and Chinese Academy of Sciences Visiting Professor for Senior International Scientists (Grant No. 2013T2G0004).

#253527 Received 6 Nov 2015; revised 10 Dec 2015; accepted 10 Dec 2015; published 25 Apr 2016
© 2016 OSA